

Radial Elastic Stiffness associated with the Bond between Steel Bars and Concrete

by James V. Cox and Hailing Yu

Department of Civil Engineering
Johns Hopkins University
Baltimore, MD 21218

Mechanical interaction between steel bars and concrete is sometimes idealized in finite element analyses as an interfacial behavior. Interface models that couple the tangent and normal responses can produce both pull-out and splitting failures. The ribs' wedging effect is represented by radial dilation of the interface, which is composed of inelastic dilation and elastic contraction (representing local elastic deformations). The effective radial elastic stiffness of the interface is related to reduced contact conditions which it accurately characterizes for a simple splitting model. A model (based upon a concrete wedge on the rib face and experimental data) is presented for estimating the contact length; it predicts the concrete wedge size and other parameters qualitatively consistent with experimental results. Variation in elastic stiffness (due to differing contact conditions) is incorporated into an interface bond model, and the predicted radial responses of selected bond specimens are improved by the more detailed treatment.

Keywords: reinforced concrete, bond, interface, contact, elastic modulus, modeling, finite element modeling, splitting, longitudinal cracking.

James V. Cox is an Assistant Professor in the Civil Engineering Department at Johns Hopkins University. He is a member of ACI Committee 408, Bond and Development of Reinforcement and of the ASCE Engineering Mechanics Division, Committee on Inelastic Behavior. His recent research has been in the area of modeling the bond behavior of steel and FRP reinforcement.

Hailing Yu is a Ph.D. student in the Civil Engineering Department at Johns Hopkins University. Her research addresses modeling the effects of mechanical interlocking between reinforcing bars and concrete.

INTRODUCTION

General models for the behavior of reinforced concrete require models for the constitutive materials and for their mechanical interaction – commonly called *bond*. “Bond models” that can be used in finite element analyses (FEA) have been proposed at various scales (see e.g., Cox and Herrmann 1998 and McCabe and Pantazopoulou 1998 for more details), two of which are depicted in Fig. 1. Usually at the smallest scale (“rib-scale” analyses) the geometry of the surface structure (i.e., ribs or deformations) of the bar is explicitly modeled, and an objective of the analysis is to examine the underlying mechanisms that produce the observed bond behavior (e.g., Ingraffea et al. 1984, Ozbolt and Eligehausen 1992; and Darwin et al. 1994). In “bar-scale” analyses the bar-concrete interface is idealized by a cylindrical shape, and thus the surface structure of the bar is not explicitly modeled. At both of these scales the bar is represented as a solid (i.e., not an axial rod), but at the bar-scale the effects of the local mechanical interaction must be accounted for indirectly. Bar-scale models can be classified by how this mechanical interaction is represented: (1) by an increased compliance of the concrete matrix adjacent to the

bar, or (2) by an increased compliance of the concrete-bar interface (e.g., De Groot et al. 1981 and Cox and Herrmann 1998). The first approach is simpler but generally does not reproduce the wedging effects of the ribs and thus can only simulate pull-out failures. The second approach (the *interface idealization*) is addressed in this paper since it can potentially simulate both pull-out and splitting failures. (For brevity, the term “bar-scale model” in the remainder of the paper will only refer to interface idealizations.) While bar-scale models do not explicitly model the underlying mechanisms that produce the observed bond behavior, they are potentially amenable to the analysis of structural components.

This paper will address an important aspect of bar-scale models that are based upon an interface idealization – the radial elastic stiffness associated with the interface. The radial elastic stiffness is important because it can have a significant affect upon the prediction of splitting failures. In some applications of interface models, the interface stiffness does not have a physical interpretation; for a bar-scale bond model the interface stiffness can be associated with the local elastic deformation that occurs between the ribs and adjacent concrete, which is not explicitly modeled at this larger scale. To better define the radial elastic stiffness of the interface, the idealizations associated with a bar-scale model are further described below.

Bar-scale idealizations

The interface idealization of bond can be described in terms of two simplifications (Cox and Herrmann 1998). The first is the homogenization (or smoothing) of the interface traction distribution and the simplification of the interface geometry. Consider a state where no adhesion remains between the bar and the concrete and thus mechanical interlocking dominates the bond behavior. Fig. 2 presents close-up views (constant q) of an axisymmetric surface structure and the corresponding cylindrical idealization, with the z -axis corresponding to the axis of the bar. Fig. 2[a] presents a schematic of the radial component of the interface traction acting on the concrete, sometimes called the “splitting or bursting force,” for a *unit surface element* consisting of the complete bar surface for one cycle of the rib geometry. In this case, the ribs are assumed to be perpendicular to the bar's axis, so the length of the unit surface element is the rib spacing (s_r). Fig. 2[b] presents a schematic of the radial component of the interface traction acting upon the concrete for a bar-scale idealization. The bar-scale idealization will produce a continuous traction distribution that is smoother than but statically equivalent over a unit surface element to the actual traction distribution. For example, the uniform distribution of s shown in Fig. 2[b] would be the bar-scale idealization of a periodic traction distribution as depicted in Fig. 2[a] for a single interval. Though not depicted in Fig. 2, the actual interface geometry changes with concrete crushing and cracking.

The second simplification, unique to interface idealizations, addresses the deformation of a unit cell of the *bond zone* – the local concrete region that behaves inelastically due to the mechanical interaction. Figs. 2[c] and 2[d] give schematics of the deformation of the actual unit cell versus the deformation of the same unit cell in the bar-scale model. d_n denotes the elastic extension of the interface (d_n in Fig. 2[d] is negative). For the two unit cells, note the difference in the distribution of the radial displacement. The elimination of the surface structure and the corresponding traction concentrations produces a different response in the concrete, even for a “perfect matrix model.” In this paper, the objective is to partially account for the effects of these simplifications upon the prediction of splitting the adjacent concrete.

The remaining sections of the paper present: (1) research significance, (2) an overview of the interface model and validation problems that motivated the study, (3) a key result from a recently obtained analytical solution and a brief description of how the analytical solution can be used to determine the equivalent elastic modulus of the interface idealization, (4) a demonstration of how the elastic modulus can be used to model the effects of contact conditions upon splitting, (5) a simple model for estimating contact conditions, (6) an improved radial elastic idealization for a bar-scale bond model, and (7) a brief discussion and conclusions.

RESEARCH SIGNIFICANCE

A bond model for FEA that can predict pull-out and splitting failures in structural components could be combined with experimental studies to better understand the progressive failure of structural components and used to calibrate configuration dependent bond models applicable to large scale structural analysis. The bond model discussed in this paper can potentially meet these needs (McCabe & Pantazopoulou 1998), yet information on the radial component of the mechanical interaction is lacking. An analytical solution (Cox and Yu 2000) and selected experimental results (Malvar 1992) are the basis for an improved radial elastic component to the model – a key toward predicting the extent of longitudinal cracking caused by “bond interaction.”

BOND MODEL OVERVIEW

The analysis presented in this study could be applied to bar-scale, interface models in general. A brief overview of the mathematical form of a particular bond model (Cox and Herrmann 1998) is presented since validation of the model by Cox and Herrmann (1999) motivated this study, and some of the findings of the current study will be demonstrated with this model. This bond model, combined with specimen models, reproduced the experimental results from six different studies with acceptable accuracy using a single calibration. Only four physical parameters are needed to apply the model: the concrete's elastic modulus and tensile strength and the bar diameter and rib spacing. The model was formulated within the mathematical framework of elastoplasticity, so the model components to be defined were the generalized stresses and strains, elastic moduli, yield criterion, and flow rule. The generalized strains for the bar-scale model are defined to be the tangent and normal displacements (\mathbf{d}_t and \mathbf{d}_n , respectively) of the concrete relative to that of the bar interface nondimensionalized by the bar diameter (d_b). The generalized stresses are the smoothed tangent and normal components of the interface tractions (τ and σ respectively), often called the *bond* and *splitting* stresses. The generalized stresses and strains are thus defined as

$$\mathbf{Q} = (\mathbf{t} \quad \mathbf{s}) \text{ and } \mathbf{q} = \frac{1}{d_b} (\mathbf{d}_t \quad \mathbf{d}_n) \quad (1a,b)$$

where the tangent and normal directions correspond to the z - and r -directions, respectively, and the relative displacements are defined for points on the interface that are coincident in the undeformed state.

For monotonic loading the evolution of the yield surface is characterized by a single measure of the internal state, the bond zone *degradation*, defined as

$$d = \min\left(\frac{\mathbf{d}_t^p}{s_r}, 1\right) \quad (2)$$

where \mathbf{d}_t^p is the plastic slip and s_r is the rib spacing. The yield criterion for the model is of the form

$$\frac{\mathbf{t}}{f_t} = C(d)F\left(d, \widehat{\mathbf{S}}(d) - \frac{\mathbf{s}}{f_t}\right) \quad (3)$$

where f_t denotes a measure of the concrete tensile strength; C is the isotropic hardening and softening function; and $\widehat{\mathbf{S}}$ is the kinematic softening function.

An additive decomposition of the generalized strains, and thus of the relative displacements, is adopted such that

$$\mathbf{q} = \mathbf{q}^e + \mathbf{q}^p \quad (4)$$

where \mathbf{q}^e and \mathbf{q}^p denote the generalized elastic and plastic strain components, respectively. The generalized plastic strains are defined by the flow rule which is of the form

$$\{\dot{\mathbf{q}}^p\} = \mathbf{I} \begin{Bmatrix} \text{sgn}(\mathbf{t}) \\ g(\mathbf{s}, d) \end{Bmatrix} \quad (5)$$

where \dot{l} denotes the consistency parameter. The kinematic behavior of the ribs wedging under the concrete, and other related effects, are characterized in the flow rule by a radial dilation. Since the rate of plastic slip has a magnitude of \dot{l} , g denotes the rate of plastic dilation (q_2^p) with respect to plastic slip. One important experimental observation characterized by the flow rule is that the rate of radial dilation decreases with confinement stress ($-\mathbf{s}$). For details on the mathematical form of $g(\mathbf{s}, d)$ see Cox (1994).

The elastic component of the model is addressed here. While the elastic moduli seem like a relatively simple component of the model, they can have a strong effect on both the predicted response and the numerical implementation. For the original model (Cox and Herrmann 1998) the elastic response under monotonic loading was characterized by the following incremental moduli

$$\mathbf{D}^e = E_c \begin{bmatrix} 0.1 & -0.0012 \operatorname{sgn}(d_i) \\ -0.0012 \operatorname{sgn}(d_i) & 0.04 \end{bmatrix} \quad (6)$$

where $\mathbf{Q} = \mathbf{D}^e \mathbf{q}^e$, $\operatorname{sgn}(0) \equiv 0$, and E_c is Young's modulus of the concrete. Magnitudes of D_{11}^e and D_{22}^e were obtained principally from experimental data (Cox 1994). The elastic response in the model is attributed primarily with the local interaction of the ribs and adjacent concrete, which is consistent with the observed variation of the "tangent elastic response" with rib geometry.

Consider a few important observations that motivated the current study:

(1) The ability of a bond model to predict splitting failures is important toward predicting the progressive failure of structural components. For this model, the wedging action of the ribs is represented by the radial dilation of the interface. The flow rule produces a radial dilation, which prior to splitting will increase the confinement stress resulting in elastic contraction of the interface (as Fig. 2[d]). Therefore, D_{22}^e is important in the prediction of the radial response which can produce splitting failures.

(2) The value of D_{22}^e was obtained from calibration since an experimental or analytical basis for its magnitude was lacking. If D_{22}^e can be attributed to the rib-concrete interaction, its value should vary with the contact conditions. Two unpublished tests of Malvar suggest that the elastic radial response becomes more compliant with radial dilation. Furthermore, Malvar (1992) performed bond tests at different levels of confinement stress applied to the outer surface of a small cylindrical specimen, and the length of the concrete wedge that formed on the front of the rib face increased with the confinement stress.

These two points are consistent with the following two validation results that partially motivated this study.* First consider the radial response predicted by the model for the tests of Malvar (1992). An axisymmetric finite element (FE) model of the specimen that incorporated the bond model gave acceptable predictions of bond stress vs. slip but under predicted the radial response. Fig. 3 presents bond stress vs. radial dilation for three levels of confinement stress, where the radial dilation corresponds to the radial displacement at the outer surface of the cylindrical specimen. Reduction in accuracy with increasing $-\mathbf{s}$ can be attributed to excessive elastic compliance of the interface.

A validation result for the tests of Shima et al. (1987) also suggests that the radial response needs further examination. Fig. 4 shows the predicted radial dilation along the embedment length at the loading level at which the model first predicts the bond zone is damaged along the entire embedment length. The contraction near the free end of the specimen is physically unrealistic, indicating that the value of D_{22}^e is too small in this end region. The region has experienced little plastic slip so there is likely to be full contact between the bar and the concrete – not merely contact at the ribs. If D_{22}^e were defined to account for contact conditions along the

* Several validation results were presented by Cox and Herrmann (1998), but this paper only examines the two results that suggested the radial elastic response needed further investigation.

interface, the model could potentially predict locally higher generalized stresses near the free end, consistent with Shima et al.'s experimental data.

Apparently how D_{22}^e should change with contact conditions has not been investigated for the bond problem. Among the sources for increased compliance are microcracks near the rib-concrete interface, macrocracks (e.g., splitting cracks), and a reduction in the contact area. The next section will first focus upon the local elastic effects of reducing the contact area independent of the “material damage.” Subsequently the effect of local crushing upon the contact area will be represented using a simple model that accounts for the deposition of crushed concrete upon the rib faces.

ANALYTICAL MODEL FOR REDUCED CONTACT EFFECTS

A few simplifications are adopted to obtain an analytical solution for the effects of reduced contact. The actual problem might have a geometry as depicted in Fig. 2[c]. A cylindrical idealization of the interface geometry is adopted, and the actual tractions are projected onto the cylindrical surface, accounting for the change in area. Unlike the bar-scale model this idealization does not “smooth out” the interface tractions. Furthermore, it is assumed: (1) that \mathbf{s} is uniform, and (2) that the corresponding actual tractions vary periodically over each unit surface element (s_r) and are symmetrically distributed about the center of each unit surface element. Boundary conditions are assumed such that the model can address the behavior of a single unit cell of a cylindrical domain as depicted in Fig. 5[a], and the elastic properties of the concrete are assumed to be homogeneous and isotropic.

The definition of the radial elastic modulus follows from the definition of *equivalence* between the idealized “rib-scale problem” (Fig. 5[a]) and the corresponding “bar-scale” idealization (Fig. 5[c]). Common to all bar-scale models the traction distributions are assumed to be “statically equivalent.” Since the actual traction distribution is unknown it is convenient to define an *equivalent problem* in which the traction is uniform over an *equivalent contact length* (Fig. 5[b]). The tractions are related by

$$\int_{-s_r/2}^{s_r/2} t_N dz = \tilde{t}_N \tilde{L}_t = \mathbf{s} s_r \quad (7)$$

where t_N and \tilde{L}_t are the *equivalent traction* and *contact length*, respectively. The equivalent traction and contact length are not uniquely defined by static equivalence alone, nor is the radial elastic modulus, so another requirement is needed. Since the elastic strain energy stored in the concrete is available for driving longitudinal cracks, the additional requirement for “problem equivalence” is defined as: two “equivalent problems” will store the same amounts of elastic strain energy. For a particular traction distribution (t_N), the quantities t_N , \tilde{L}_t and D_{22}^e can be uniquely determined by equating the strain energy stored in each of the respective problems. Solution of the problem depicted in Fig. 5[a] was previously presented by Cox and Yu (2000). A brief description of the analytical solution is presented below merely to establish key nomenclature. Additional detail is available in Appendix I, or in Cox and Yu (2000).

Description of analytical solution

The governing equations of linear isotropic elasticity were solved by expressing the nonzero displacement components as

$$\mathbf{u}_t(r, z) = \bullet \sum_{n=0}^{\infty} \mathbf{n}_{tn}(r) \mathbf{F}_{cn}(z), \quad \mathbf{u}_z(r, z) = \bullet \sum_{n=1}^{\infty} \mathbf{n}_{zn}(r) \mathbf{F}_{sn}(z) \quad (8a,b)$$

where

$$F_{cn}(z) = \begin{cases} \frac{1}{\sqrt{s_r}}, & n=0 \\ \frac{\cos(zw_n)}{\sqrt{s_r/2}}, & n>0 \end{cases}, \quad F_{sn}(z) = \frac{\sin(zw_n)}{\sqrt{s_r/2}}, \quad w_n = \frac{2pn}{s_r} \quad (8c-e)$$

The coefficient functions are given by

$$\mathbf{n}_m(r) = \langle \mathbf{u}_r(r, z), \mathbf{F}_{cn}(z) \rangle, \quad \mathbf{n}_{zn}(r) = \langle \mathbf{u}_z(r, z), \mathbf{F}_{sn}(z) \rangle \quad (9a,b)$$

where $\langle \mathbf{a}, \mathbf{b} \rangle \equiv \int_{-s_r/2}^{s_r/2} \mathbf{a} \mathbf{b} dz$. Solution of the governing equations gave expressions for the coefficient functions for the displacement components in terms of modified Bessel functions. Expressions for the stresses could also be obtained in terms of $\{\Phi_c\}$ and $\{\Phi_s\}$ (Eqs. 8c-e). Traction boundary conditions on the inner and outer surfaces could be used to solve for unknown constants and to do so required the load to be expressed in terms of the normalized cosine functions as

$$t_N(z) = \sum_{n=0}^{\infty} \mathbf{a}_n \mathbf{F}_{cn}(z) \quad (10a)$$

where the \mathbf{a} 's are given by

$$\mathbf{a}_n = \langle \Phi_{cn}(z), t_N(z) \rangle \quad (10b)$$

The exact solution can be expressed analytically, but the expressions are lengthy and thus are omitted for brevity.

The $n=0$ term of the solution corresponds to the uniform traction case (i.e., \mathbf{s}), thus the remaining terms characterize the difference in response in *problems a* and *c* (omitting the contribution of the interface). This is illustrated by an example that was previously used to verify the correctness of the analytical solution. A unit cell of the bond specimen of Malvar (1992) is examined: $r_i = 9.525$ mm, $r_o = 4 r_i$, $L_t = 1.587$ mm, $s_r = 12.8$ mm, $E = 38700$ MPa and $\nu = 0.17$. The normal traction is uniform with a magnitude of s_r/L_t MPa (i.e. corresponds to $\mathbf{s} = -1$ MPa). Fig. 6 shows a subset of the FE solution for \mathbf{s}_{rr} over half of the unit cell due to an applied normal traction of $\bar{t}_N - \mathbf{s}$. To emphasize that significant differences in the responses of the two problems are “localized” near the interface, values are only shown when $|\mathbf{s}_{rr}| > |\mathbf{s}|/100$. By Eq. (7), the resultant radial force due to $\bar{t}_N - \mathbf{s}$ is zero, so by Saint-Venant’s principle the “local nature of the response” is expected. Note that the solution for the local response was essentially independent of r_o for $r_o > 2r_i$.

With an analytical solution, the problem of determining the equivalent elastic modulus of the interface, to characterize this local behavior, can now be addressed. The result shown below is similar to that derived by Cox and Yu 2000, but in this study the elastic modulus relates \mathbf{s} to the generalized strains of the bond model. (A more detailed overview is available in Appendix II.)

Equivalent elastic modulus

We previously defined *equivalent problems* as those that store the same amount of elastic strain energy and have “statically equivalent” traction distributions. The strain energy stored in an elastic unit cell is equal to the work done by the traction t_N . Therefore, the approach is to simply use the analytical solution to compute the work done by the interface tractions in *problems a* and *c*, and then equate the works to determine an expression for D_{22}^e . The elastic modulus can be written as

$$D_{22}^e = \frac{2E_c}{-\sum_{n=1}^{\infty} \left(\frac{\mathbf{a}_n}{\mathbf{a}_0}\right)^2 h(\mathbf{w}_n r_i, r_i/r_o, \mathbf{n})} \quad (11)$$

where $\mathbf{n}_m(r_i)$ is expressed in the symbolic form

$$\mathbf{n}_m(r_i) = \frac{\mathbf{a}_n r_i h(\mathbf{w}_n r_i, r_i/r_o, \mathbf{n})}{E_c} \quad (12)$$

and h is a dimensionless function.

Assume that the rib geometry scales with d_b , which is approximately true for standard steel bars. Furthermore, assume that (for a given load level) the scaling of the rib geometry will scale the traction distribution accordingly. Then both $\mathbf{a}_n/\mathbf{a}_0$ and $\mathbf{w}_n r_i$ are independent of d_b . If $r_o > 2r_i$, then D_{22}^e is essentially independent of d_b , and the dependence of the elastic response upon d_b is given by the definition of the generalized elastic strains (Eq. 1) – originally motivated by the characterization of bond test data (Morita and Fujii 1985). As expected the elastic modulus varies proportionately with Young's modulus. Variation of the elastic modulus with Poisson's ratio (over a representative range) was shown to be negligible (Cox and Yu 2000).

The denominator of Eq. (11) gives a direct measure of the effect of having a nonuniform traction distribution. As previously noted, the zero term of Eq. (8a) gives the displacements of the unit cell for a uniform traction distribution. All of the other terms in the series expansions account for the deviation from a uniform distribution, are "statically equivalent to a zero traction," and thus in combination (in a Saint-Venant sense) represent the local response.

As previously discussed there is significant motivation for including the effects of contact in the elastic response even though there also are several uncertainties. The paper will briefly consider two factors related to the contact between the ribs and the concrete: contact length and traction distribution.

Fig. 7 shows the variation of the elastic modulus with respect to contact length and for two different traction distributions over L_t (uniform and cosine). Over the contact length, the cosine distribution is given by $t(z) = t_{max} \cos(z\pi/L_t)$, where t_{max} denotes the maximum traction value. The properties correspond to a unit cell of the Malvar (1992) bond specimen. These analytical results support the postulate that the stiffness of the interface should decrease with a reduction in the contact length. The results also indicate that the effect of the traction distribution increases with the contact length. As previously noted, since both the contact length and traction distribution are unknown it may be simpler to consider an equivalent system with a constant traction distribution over the contact length. Equivalent systems will store the same amounts of elastic strain energy, and thus will have the same elastic modulus. As an example (see the "box" on Fig. 7), a cosine distribution with a contact length of $s_r/2$ will have an equivalent contact length of about $0.38s_r$, which is intuitively consistent with the cosine distribution being more concentrated (for a fixed L_t) than a constant distribution associated with the same "radial force."

For the uniform traction distribution over the contact length, $D_{22}^e \rightarrow \infty$ as $L_t \rightarrow s_r$, since *problems b* and *c* are the same under these conditions. In contrast, for the cosine traction distribution D_{22}^e approaches a finite value for full-contact conditions. That is, even if full contact exists along the interface any "smoothing" of a nonuniform traction distribution requires a finite elastic modulus for the interface if the two systems are to store the same amount of elastic strain energy.

EFFECT OF ELASTIC MODULUS ON LONGITUDINAL CRACKING

The definition of D_{22}^e was motivated by the need to predict splitting failures when using bar-scale models. The effects of longitudinal cracking in the concrete cover upon the bond response are commonly idealized by thick-walled cylinder models that approximate the effects of longitudinal cracking in the context of an axisymmetric analysis. Tepfers (1979) initially

considered a concentric cylinder model in which the hoop stress in the concrete was released upon reaching its tensile strength. Several other models have been proposed that adopt a fictitious crack model (Hillerborg et al. 1976) to account for the fracture energy of the longitudinal cracks. Noghabai (1995) gives a detailed review of these types of models. In all cases, a uniform internal pressure is assumed to act upon the concrete cylinder. An axisymmetric idealization is adopted in this study that uses the general approach of Rots (1988) to account for the longitudinal cracking in a FE model. Each crack is idealized as being planar with a process zone of infinitesimal thickness and finite length. The crack opening contributes to the apparent hoop strain and the material between cracks is treated as linear elastic. The behavior of the process zone is characterized by the following traction–crack opening relationship (Reinhardt et al. 1986)

$$\frac{s_{cr}}{f_t} = (1 + C_1 \hat{w}^3) \exp(-C_2 \hat{w}) - (1 + C_1) \exp(-C_2) \quad (13)$$

where \hat{w} is the ratio of the opening displacement of the cohesive crack and the *critical crack opening*, w_o –the minimum crack opening for which there is no traction across the crack, f_t is the tensile strength of the concrete, and C_1 and C_2 are model parameters. For the examples considered here: $C_1 = 2.146$, $C_2 = 6.93$, $f_t = 4.69$ MPa, and $w_o = 0.16$ mm implying the *fracture energy* is 100 J/m^2 .

To examine the effect of this axisymmetric idealization alone, σ versus $u_r(r_i)$ responses of axisymmetric models and plane strain models (having evenly spaced cracks) of a unit cell of the Malvar (1992) bond specimen are compared (Fig. 8). Fig. 9 shows the results for two, three, and four cracks. The results reflect the expected trend that the accuracy of the axisymmetric idealization increases with the number of cracks. Depending upon the bond specimen, the number of longitudinal cracks that reach the surface often varies between two and four. While the axisymmetric idealization has limitations, it still serves as an acceptable model in which to examine the effects of the contact conditions.

The derivation of D_{22}^e was based upon linear elastic behavior. Now consider how effective Eq. (11) is at quantifying the added compliance associated with a reduced contact area when longitudinal cracking occurs. Again a unit cell of the Malvar bond specimen is adopted for demonstration. Fig. 10 shows σ versus the average work conjugate radial displacement for the case of two, three, and four longitudinal cracks. In each case, the response for a uniform traction without additional interface compliance (i.e., $\tilde{L} = s_r$) is given for reference, and contact lengths corresponding to the length of the rib face ($s_r/L_t \approx 1/8$) and $s_r/2$ are also shown. For the reduced contact cases two results are shown: (1) a FE solution explicitly modeling the reduced contact (*problem b*), and (2) a FE solution that incorporates an interface stiffness determined from Eq. (11) (*problem c*). In each case, the two analysis results are almost identical, indicating that D_{22}^e effectively represents the effect of reduced contact area even at load levels that split the concrete cylinder.

The results also reflect a significant variation in radial displacement with contact length. For smaller effective contact lengths, the radial displacement required to split the concrete cylinder is significantly more than that given by a uniform traction. The potential importance of this result is that the radial displacement shown in these plots corresponds to the inelastic normal displacement of a bond model (e.g., d_2^p), thus the prediction of splitting failure can be significantly affected by the contact conditions. Unfortunately contact conditions are likely to vary during loading and experimental data on the contact state is lacking. To model the effects of

changing contact conditions, the elastic component of the bond model was recently modified but an analytical basis for this modification (partially presented in the previous sections) had not been developed. The next section first presents the new form of the elastic component of the bar-scale bond model. Then a simple rib-scale model, used to estimate the effect of local crushing upon the contact length, and selected experimental results were used to relate the bond model to estimates of the contact length.

RELATING CONTACT EFFECTS TO THE BOND MODEL

The key idea that motivated the analytical work of the earlier sections was that D_{22}^e should decrease with a decrease in contact area. For the bond model, it was postulated that the contact area would decrease with an increase in q_2^p ($=d_2^p/d_b$), so a strain energy function, quadratic in the elastic strains, was selected so that the generalized stresses are given by

$$\mathbf{Q} = \mathbf{D}^e(q_2^p)\mathbf{q}^e \quad (14)$$

For simplicity, since the off-diagonal moduli were very small, only the diagonal moduli are retained. The elastic response is now coupled to the plastic response (elastoplastic coupling), but initially this coupling is considered for the radial component alone, i.e.,

$$\mathbf{D}^e(q_2^p) = \text{diag}(D_{11}^e, D_{22}^e(q_2^p)) \quad (15)$$

A simple affine relationship was adopted between the elastic compliance modulus for the radial response and q_2^p , i.e.,

$$\left(\frac{D_{22}^e}{E_c}\right)^{-1} = k_1 + k_2(q_2^p) \quad (16)$$

where k_1 and k_2 were calibration parameters.

Relating Eq. (16) to the previous analytical results will indicate the adequacy of this simple model and potentially allow k_1 and k_2 to be determined from the analytical solution and experimental data. To apply the analytical solution requires the contact length (L_t – a “rib-scale quantity”) to be related to the radial plastic strain (q_2^p – a “bar-scale quantity”). Change in the contact length is a direct result of deformation, and for steel bars that have not yielded, most of this deformation is associated with failure of the concrete. While q_2^p conceptually includes the effects of inelastic deformations of the concrete, the effects of concrete deformation considered in the following development are limited to the recognition that a wedge of damaged concrete has been found to accumulate on the face of the rib (e.g., Lutz and Gergely 1967). The experimental data of Fig. 3 shows that (1) most of the radial dilation occurs near the failure state (\mathbf{t}_{max} in this case), and (2) the radial dilation (for bars with normal ribs) remains almost constant during much of the bond stress softening response. The maximum dilation is critical to predicting the splitting response so the simple model discussed below is only used to relate L_t to q_2^p at the state when the maximum radial dilation first occurs.

Contact length estimate

A simple rib-scale model for relating L_t to q_2^p is adopted that includes a concrete wedge in front of the rib. The geometry is depicted in Fig. 11. The surface of the concrete wedge will be referred to as the *actual interface surface* in the following description. From geometry

$$p_r = h_r / \tan f \quad (17a)$$

$$d_2^p = h_r - L_t \tan f \quad (17b)$$

where p_r is the projected length of the actual surface area onto the cylindrical core of the bar, and f is the angle of inclination of the actual interface surface with respect to the axis of the bar.

Except for the existence of the concrete wedge, the depicted geometric model ignores the local deformation of the concrete and thus is only valid if $d_2^c \ll d_2^p$.*

The interface tractions resulting from the mechanical interaction between the concrete and ribs have so far been idealized in two ways: smoothed (or homogenized) over the unit surface element (Fig. 2[b]), and projected onto a cylindrical idealization of the bar surface (Fig. 5). The traction components on the actual interface of the concrete (\mathbf{s}_w and \mathbf{t}_w) are schematically depicted in Fig. 12[a] in a local tangent-normal coordinate system; the alternative description, used in the previous section, is shown in Fig. 12[b]. (For simplicity uniform traction components are shown, but a nonuniform distribution will also be considered.) It is sufficiently accurate for standard steel bars to assume that $q_2^p \ll 1$ and $h_r \ll d_b$. With these assumptions, static equivalence over a unit surface element of the average (over L_t) actual traction components ($\bar{\mathbf{s}}_w$ and $\bar{\mathbf{t}}_w$) with the homogenized traction components yields the following relationships

$$\bar{\mathbf{s}}_w = \cos f (\mathbf{s} \cos f - \mathbf{t} \sin f) s_r / L_t \quad (18a)$$

$$\bar{\mathbf{t}}_w = \cos f (\mathbf{s} \sin f + \mathbf{t} \cos f) s_r / L_t \quad (18b)$$

Now consider the stress state of the concrete in the contact region. One might consider a multiaxial failure criterion to determine the stress state in the concrete, but there are several obstacles to this approach: (1) the actual tractions are unknown, (2) other stress components are unknown, (3) material properties near the bar are unknown (e.g., due to aggregate packing) and vary spatially, and (4) common macroscopic failure criterion for concrete are not directly applicable at this scale. For the states where the maximum dilation first occurs we assume that Coulomb friction can be used to relate \mathbf{s}_w and \mathbf{t}_w and that \mathbf{s}_w reaches a maximum magnitude at this state. The friction condition governing slip along the actual interface is given by

$$|\bar{\mathbf{t}}_w| \leq m(-\bar{\mathbf{s}}_w) \quad (19)$$

where m is the coefficient of friction. Note that this relationship has been commonly used in rib-scale analyses to relate the interface traction components at each point (e.g., Tholen and Darwin 1996).

Because of the previously noted difficulties, a semi-empirical approach is taken to estimate the maximum magnitude of \mathbf{s}_w . A rib-scale FE model of the Malvar specimen is used to calculate the value of \mathbf{s}_w on the rib face closest to the loaded end for the various confinement states. The value of \mathbf{s}_w corresponding to initial nonlinearity in the bond stress-slip response is assumed to be the result of local crushing that will contribute to the formation of a concrete wedge on the face of the rib (e.g., Lutz and Gergely 1967). Fig. 13 shows one representative result of the three tests considered. The nonlinearity occurred approximately when

$$-\bar{\mathbf{s}}_w = f_c \quad (20)$$

Combining the above relationships (Eqs. 17-20) with key experimental data for the three test results shown in Fig. 3, estimates of the contact length are obtained. Table 1 gives the empirical data obtained from the three tests having normal ribs (tests 6, 8, and 10) for the state where the maximum dilation first occurs; consistent with the above assumption, we let $d_2 \approx d_2^c$. The relevant properties (that were not previously given) are: $h_r=1.3$ mm, $p_{ro}=1.587$ mm, and $f_c=38.4$ MPa. Eqs. (17-20) yield six relationships in six unknowns (L_t , p_r , \mathbf{f} , \mathbf{t}_w , \mathbf{s}_w , m). Treating m as an unknown allows the consistency of the above relations to be examined. Assuming that both sliding and crushing occur at the maximum dilation point, Ineq. (19) “becomes an equality.” The nonlinear equations can now be analytically solved as follows: (1) Eqs. (17b, 18a, 20) give L_t , \mathbf{f} , and \mathbf{s}_w ; Eq. (18b) gives \mathbf{t}_w ; Eq. (19) gives m and Eq. (17a) gives p_r .

* This assumption was later revisited, by using the calculated D_{22}^c to estimate d_2^c . d_2^p of Eq. (17b) was replaced by d_2 and D_{22}^c was recalculated and found to differ by less than 1.5 percent.

Results

Results are shown in Table 2. The estimated value of m is surprisingly consistent for the simple model and is close to the average experimental values obtained by several researchers: 0.56 (Idun and Darwin 1999), 0.53 (Cairns and Abdullah 1994), and 0.57 (Rabbat and Russell 1985).

If m is now taken to be 0.55 and d_2^p is treated as an unknown, the predicted values for the maximum d_2^p shown in Table 3 are reasonably accurate. Using these calculated values of L_t , the compliances are determined from Eq. (11), or obtained graphically from Fig. 7. The compliance values given in Table 3 correspond to cosine traction distributions. Note that the predicted variation in the compliance is one order of magnitude.

The last step is to relate the variation in compliance to the simpler model function, Eq. (16). Fig. 14 shows the least square fits of the affine model to the data obtained using the analysis described above; two traction distributions over the contact region are considered – uniform and cosine. For both traction distributions, the data obtained with the local model is fit accurately by a line and the slope of the line (k_2) is not strongly dependent upon the traction distribution. The model for the uniform distribution is not physically meaningful for very small q_2^p , since it predicts a nonpositive definite elastic response. For this study, the model based on the cosine distribution is adopted; the calibration parameters are $k_1=0.034$ and $k_2=27$.

Accounting for a change in the radial elastic stiffness of the interface, the bond model gives the results shown in Figs. 15 and 16, for the Malvar and Shima et al. tests, respectively. Comparison of Figs. 3 and 15 shows the radial response of the model is significantly improved. The main objective was for the model to reproduce the general behavior with acceptable maximum dilations. Further refinement of the model or its calibration would require a measure of the experimental scatter. Fig. 16 compares the original model's response to that of the model with varying elastic properties. The model now predicts that the clamping action towards the free end of the bar produces a lack of dilation rather than a penetration.

SUMMARY AND CONCLUSIONS

For an interface idealization of bond behavior the effective radial elastic modulus of the interface can be associated with local elastic deformation resulting from the mechanical interlocking between the ribs of a bar and the adjacent concrete. The key premise in obtaining the analytical expression for the elastic modulus was that “equivalent traction distributions” should produce the same amount of elastic strain energy in the constituent materials. While the analytical solution required several simplifying assumptions, it provides information on an elastic modulus for which there is apparently no experimental data. If one associates the change in traction distribution with contact between the bar and concrete, the analytical solution shows the interface stiffness should increase with the contact length. Numerical results indicate that the analytical solution for D_{22}^e also can characterize the elastic effects of reduced contact for radial forces that are large enough to split the concrete.

Through a simple model that accounts for the accumulation of a concrete wedge on a rib face and key experimental data, contact lengths were estimated and related to an interface description of bond for states in which the “splitting force” has its maximum effect (i.e., when the radial dilation is at a maximum). The predicted coefficients of friction were quantitatively consistent with existing experimental results, and the accumulation of concrete on the rib face (increasing with confinement stress) was consistent with experimental observations.

There are several issues that may merit further investigation. The effects of heterogeneous material properties (including the effects of micro-cracking) upon D_{22}^e have not been quantified. The semi-empirical approach to quantifying the local crushing failure is simple, but there are several factors that discourage a more rigorous treatment at this scale (including unknown

traction distributions and heterogeneous material properties). Further more, application of the model to bars with non-normal ribs can only be justified in a qualitative sense.

Significant improvements in the predicted radial response of a bond model were obtained by modeling the effect of changes in the estimated contact area upon the radial elastic response. Axisymmetric models of the Malvar specimen predicted the radial dilation with good accuracy, and the erroneous prediction of interface contraction with the Shima et al. specimen was eliminated. Improvements in the radial response of this type of model increases the potential of applying them to predict the behavior of structural components in which splitting and pullout failures could occur.

ACKNOWLEDGMENTS

Support for this study by the National Science Foundation (grant no. CMS-9872609), the Naval Facilities Engineering Service Center (contract no. N0024499P2444), and the Office of Naval Research are gratefully acknowledged. Miss. Kristine Bergeron helped conduct FEAs for Fig. 9.

REFERENCES

- Cairns, J., and Abdullah, R., "Fundamental Tests on the Effects of an Epoxy Coating on Bond Strength," *ACI Materials Journal*, 91(4), 1994, pp. 331-338.
- Cox, J.V. "Development of a Plasticity Bond Model for Reinforced Concrete – Theory and Validation for Monotonic Applications," *Technical Report: TR-2036-SHR*, Naval Facilities Engineering Service Center, Port Hueneme, CA, 1994.
- Cox, J.V., and Herrmann, L.R., "Development of a Plasticity Bond Model for Steel Reinforcement," *Mechanics of Cohesive-Frictional Materials*, 3, 1998, pp. 155-180.
- Cox, J.V., and Herrmann, L.R., "Validation of a Plasticity Bond Model for Steel Reinforcement," *Mechanics of Cohesive-Frictional Materials*, 4, 1999, pp. 361-389.
- Cox, J.V., and Yu, H., "A Micromechanical Analysis of the Radial Elastic Response associated with Slender Reinforcing Elements within a Matrix," *Journal of Composite Materials*, 2000, 33(23), 1999, pp 2161-2192.
- Darwin, D., McCabe, S.L., Brown, C.J., and Tholen, M.L., "Fracture Analysis of Steel-Concrete Bond," *Fracture and Damage in Quasibrittle Structures*, E & FN Spon, London, 1994, pp. 549-556.
- De Groot, A.K., Kusters, G.M.A., and Monnier, T., "Numerical Modeling of Bond-Slip Behavior," Heron, 26-1b, I.B.B.C. Institute TNO, Delft, Netherlands, 1981.
- Hillerborg, A., Mod er, M., and Petersson, P.A., "Analysis of Crack Formation and Crack Growth in Concrete by means of Fracture Mechanics and Finite Elements," *Cement and Concrete Research*, 6, 1976, pp. 773-782.
- Idun, E. K. and Darwin, D., "Epoxy-Coated Reinforcement: Coefficient of Friction and Rib Face Angle," *ACI Structural Journal*, 96(4), 1999 pp. 609-615.
- Ingraffea, A.R., Gerstle, W.H., Gergely, P., and Saoma, V., "Fracture Mechanics of Bond in Reinforced Concrete," *Journal of Structural Engineering*, ASCE, 111(5), 1984, pp. 871-890.
- Lutz, L.A., and Gergely, P., "Mechanics of Bond and Slip of Deformed Bars in Concrete," *ACI Journal*, 64, 1967, pp. 711-721.
- Malvar, L.J., "Bond of Reinforcement under Controlled Confinement," *ACI Materials Journal*, 89(6), 1992, pp. 593-601.
- McCabe, S.L., and Pantazopoulou, S.J., "Evaluation of Bond Performance in Reinforced Concrete Structures," *Bond and Development of Reinforcement*, SP-180, ACI, Roberto Leon, ed., SP 180-1, 1998, pp. 1-21.
- Morita, S., and Fujii, S., "Bond-Slip Models in Finite Element Analysis," *Proc., Japan-US Seminar on Finite Element Analysis of Reinforced Concrete Structures*, Tokyo, 1985, pp. 348-363.

Noghabai, K., "Splitting of Concrete in the Anchoring Zone of Deformed Bars," Licentiate Thesis, 26L, Div. of Struc. Eng., Luleå University of Technology, Sweden, 1995, 131 pp.

Ozbolt, J., and Eligehausen, R., "Numerical Simulation of Cycling Bond-Slip Behavior," Bond in Concrete, Proceedings of the International Conference, Riga, Latvia, CEB, 3, 1992, pp. 12.27-12.33.

Shima, H., Chou, L., and Okamura, H., "Micro and Macro Models for Bond in Reinforced Concrete," *Journal of the Faculty of Engineering*, The University of Tokyo (B), 39(2), 1987, pp. 133-194.

Tepfers, R., "Cracking of Concrete Cover along Anchored Deformed Reinforcing Bars," *Magazine of Concrete Research*, 31(106), 1979, pp. 3-12.

Rabbat, B.G., and Russell, H.G., "Friction Coefficient of Steel on Concrete or Grout," *Journal of Structural Engineering*, ASCE, 111(3), 1985, pp. 505-515.

Reinhardt, H.W., Cornelissen, H.A.W., and Hordijk, D.A., "Tensile Tests and Failure Analysis of Concrete," *Journal of the Structures Division*, ASCE, 112(11), 1986, pp. 2462-2477.

Rots, J.G., "Computation Modeling of Concrete Fracture," Ph.D. dissertation, Delft University of Technology, Delft, 1988, 135 pp.

Footnotes

Several validation results were presented by Cox and Herrmann (1998), but this paper only examines the two results that suggested the radial elastic response needed further investigation.

This assumption was later revisited, by using the calculated D_{22}^e to estimate d_2^e . d_2^p of Eq. (17b) was replaced by d_2 and D_{22}^e was recalculated and found to differ by less than 1.5 percent.

Tables for the paper:

"Modeling the radial elastic stiffness associated with
the bond between steel bars and concrete"

by James V. Cox and Hailing Yu, Members ASCE

Table 1—Experimental data

Table 2—"Contact Model" Results (m unknown)

Table 3—Elastic Modulus Predictions ($m=0.55$)

Table 1—Experimental data

	d_2^p (mm)	s (MPa)	t (MPa)
Test 6	0.512	-3.45	5
Test 8	0.135	-17.2	14
Test 10	0.029	-31	22

Table 2—“Contact Model” Results (m unknown)

	f (deg)	p_r (mm)	L_t (mm)	\bar{s}_w (MPa)	\bar{t}_w (MPa)	$m = \bar{t}_w / \bar{s}_w $
Test 6	26.4	2.62	1.59	-38.4	21.3	0.554
Test 8	10.4	7.11	6.37	-38.4	21.1	0.549
Test 10	6.57	11.3	11.0	-38.4	21.1	0.550

Table 3—Elastic Modulus Predictions ($m=0.55$)

	L_t (mm)	d_2^p (mm)	$\frac{ d_2^p - d_{2\text{exp}}^p }{d_{2\text{exp}}^p}$	$q_2^p = d_2^p / L$	E_c / D_{22}^e
Test 6	1.59	0.506	1.2%	0.0265	0.758
Test 8	6.37	0.138	2.3%	0.00724	0.240
Test 10	11.0	0.033 2	14.5%	0.00174	0.075

Figures for the paper:

"Modeling the radial elastic stiffness associated with
the bond between steel bars and concrete"

by James V. Cox and Hailing Yu, Members ASCE

Fig. 1—Two scales of bond analysis

Fig. 2—Bond model interface idealizations

Fig. 3—Average bond stress vs. radial dilation: a comparison of the original model to the data of
Malvar (1992): □ ~ rib angle of 90 degrees, and × ~ rib angle of 68 degrees

Fig. 4—Radial dilation vs. position: predictions of the original model for the Shima et al. (1987)
specimen

Fig. 5—Idealizations for the radial response

Fig. 6—FE prediction of difference in s_{rr} due to two equivalent traction distributions

Fig. 7—Variation of the elastic modulus with contact length

Fig. 8—Plane strain and axisymmetric FE models for Malvar specimen

Fig. 9—Responses of the plane strain and axisymmetric models

Fig. 10—Interface compression vs. radial dilation for Malvar unit cell

Fig. 11—Kinematic model relating contact length to plastic dilation

Fig. 12—Two descriptions of the actual interface tractions

Fig. 13—Compressive failure in Malvar Test 9

Fig. 14—Models for elastic modulus as a function of plastic dilation

Fig. 15—Average bond stress vs. Radial dilation: a comparison of the new model to the data of
Malvar (1992): □ ~ rib angle of 90 degrees, and × ~ rib angle of 68 degrees

Fig. 16—Radial dilation vs. position: predictions of the models for the [Shima et al. \(1987\)](#) specimen

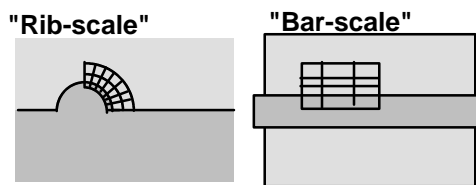


Fig. 1—Two scales of bond analysis

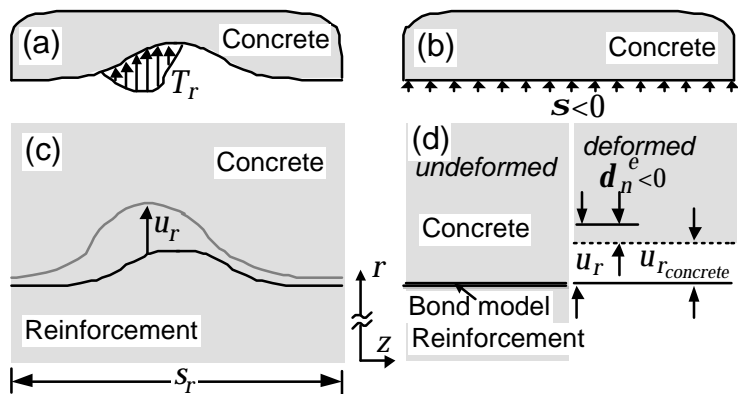


Fig. 2—Bond model interface idealizations

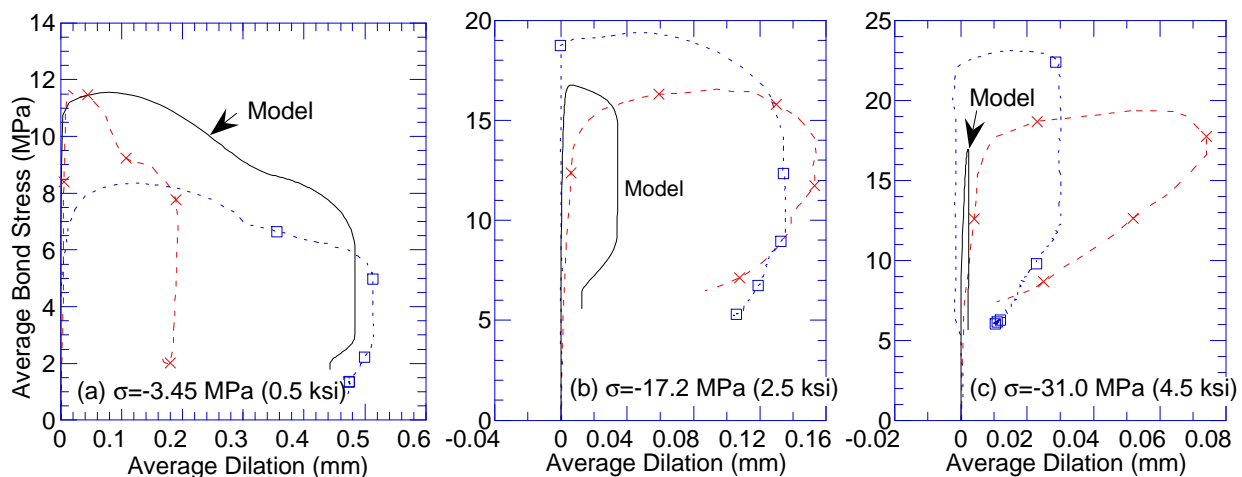


Fig. 3—Average bond stress vs. radial dilation: a comparison of the original model to the data of Malvar (1992): \square ~ rib angle of 90 degrees, and \times ~ rib angle of 68 degrees

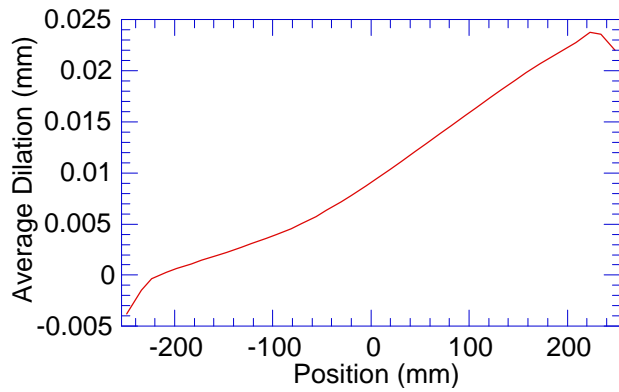


Fig. 4—Radial dilation vs. position: predictions of the original model for the [Shima et al. \(1987\)](#) specimen

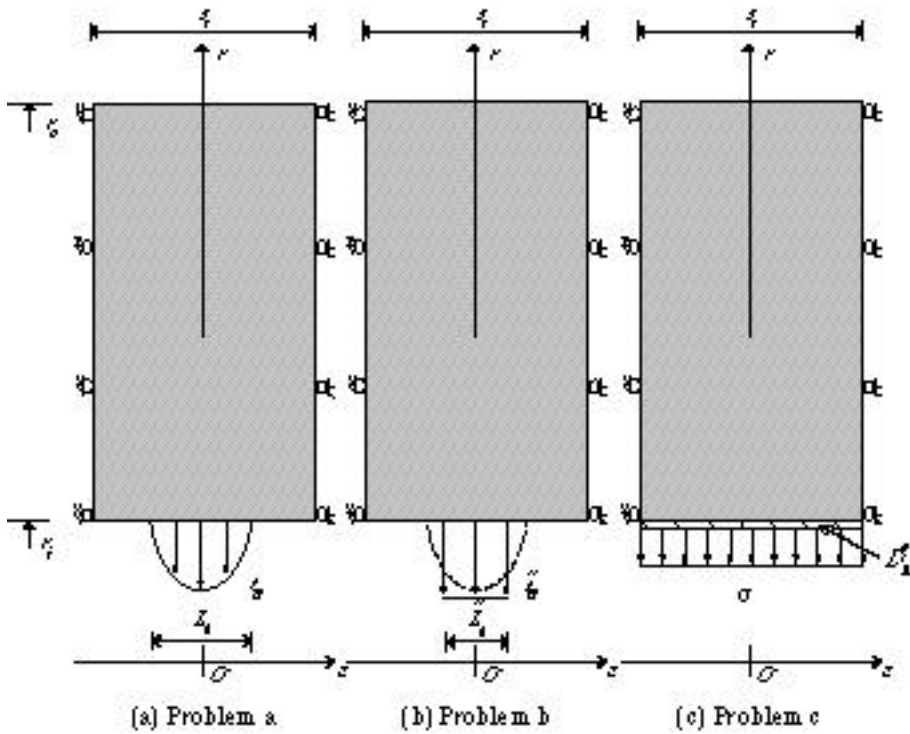


Fig. 5—Idealizations for the radial response

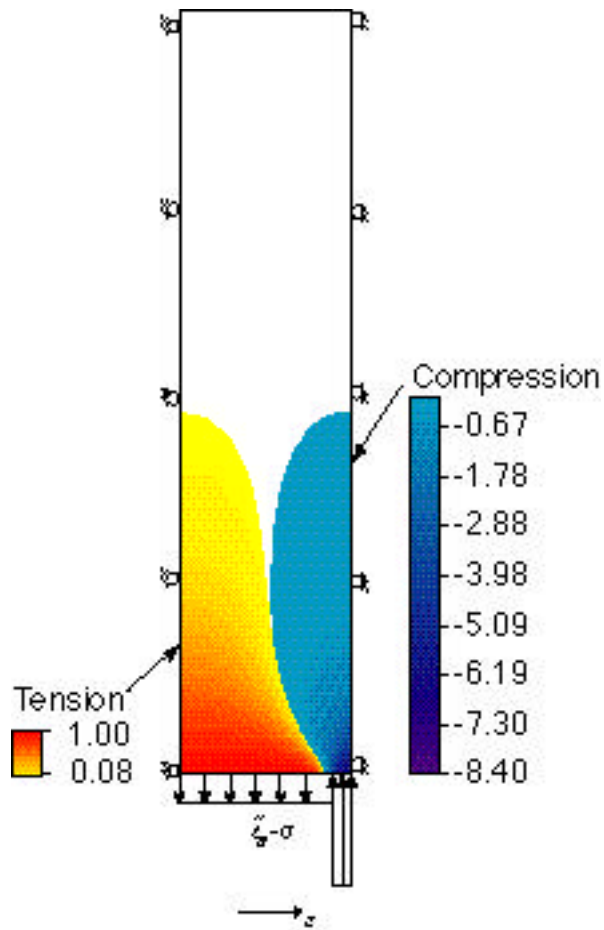


Fig. 6—FE prediction of difference in σ_{rr} due to two equivalent traction distributions

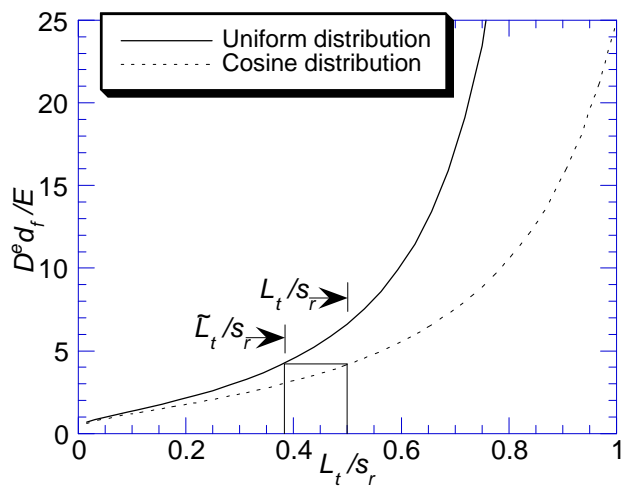


Fig. 7—Variation of the elastic modulus with contact length

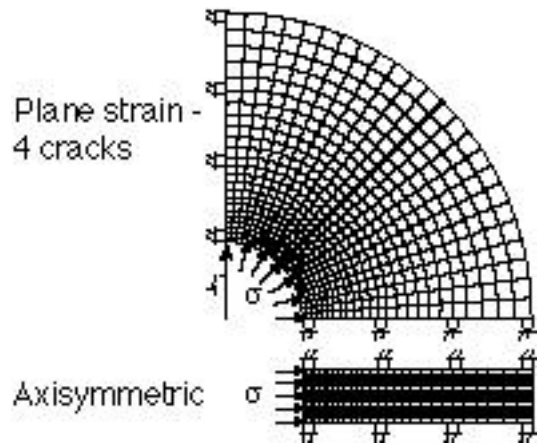


Fig. 8—Plane strain and axisymmetric FE models for Malvar specimen

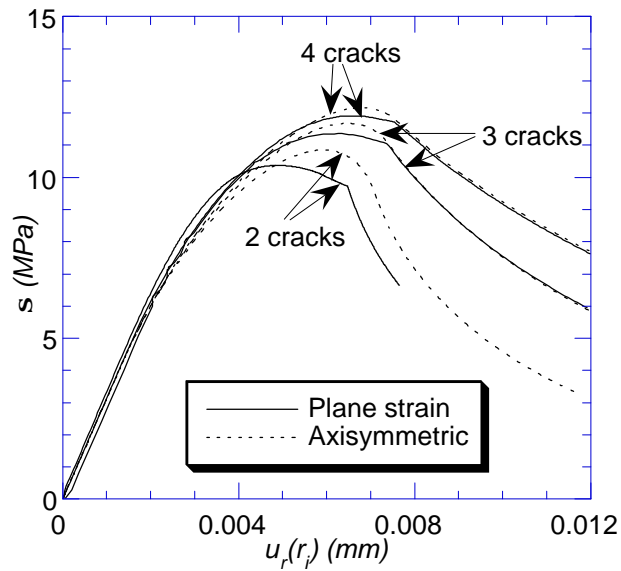


Fig. 9—Responses of the plane strain and axisymmetric models

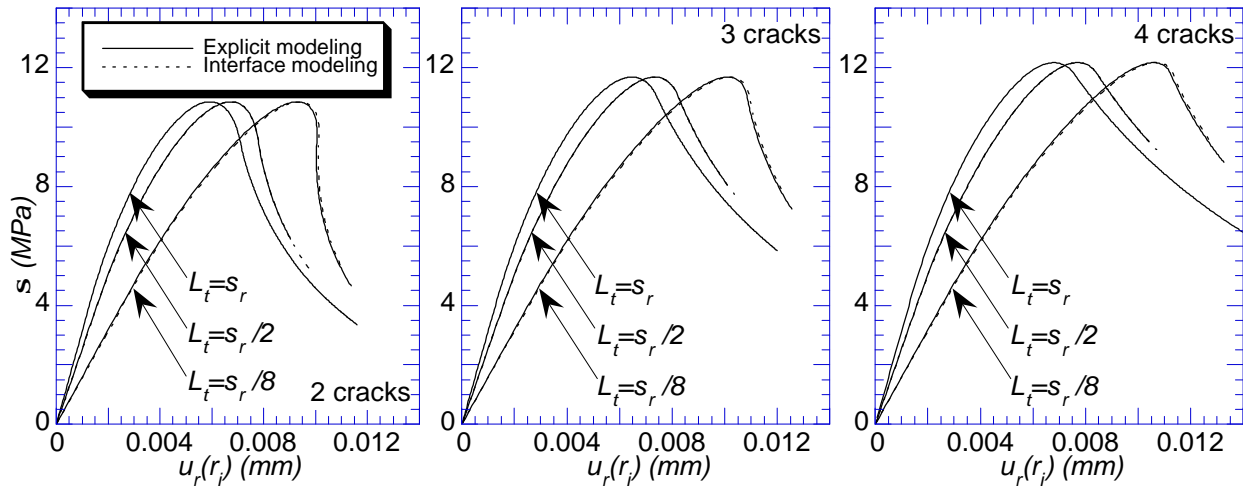


Fig. 10—Interface compression vs. radial dilation for Malvar unit cell

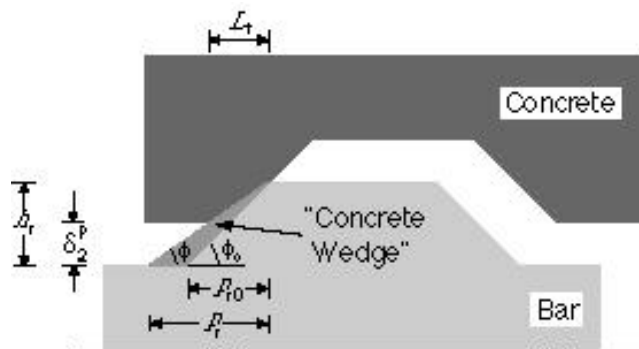


Fig. 11—Kinematic model relating contact length to plastic dilation

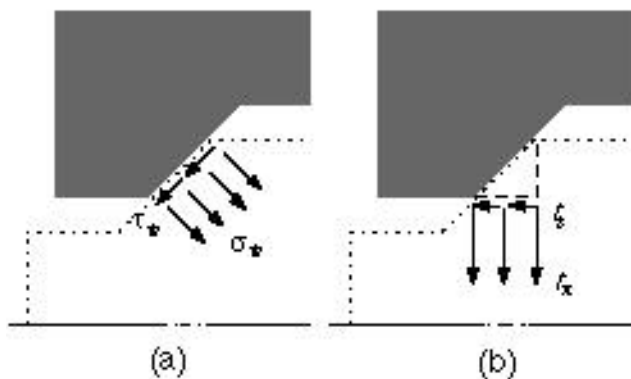


Fig. 12—Two descriptions of the actual interface tractions

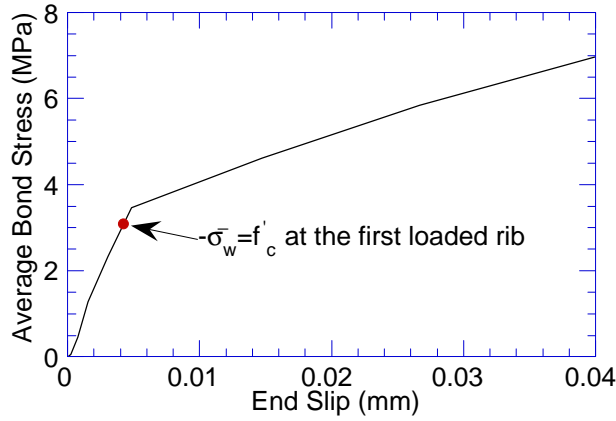


Fig. 13—Compressive failure in Malvar Test 9

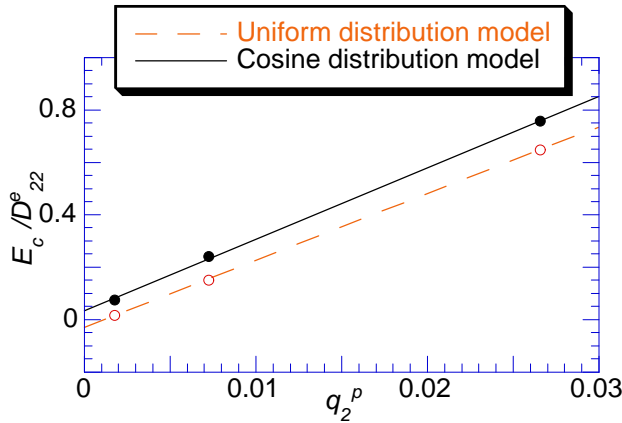


Fig. 14—Models for elastic modulus as a function of plastic dilation

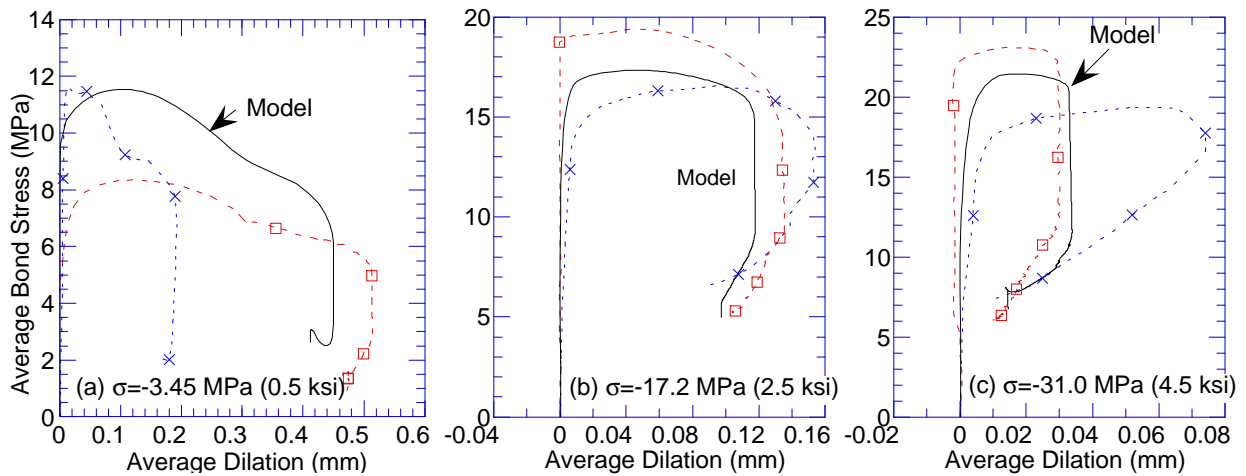


Fig. 15—Average bond stress vs. Radial dilation: a comparison of the new model to the data of Malvar (1992): \square ~ rib angle of 90 degrees, and \times ~ rib angle of 68 degrees

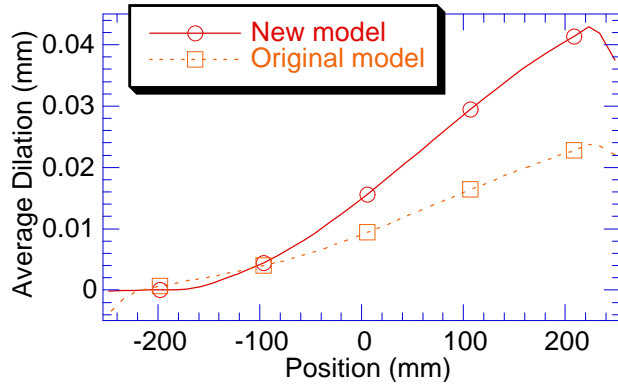


Fig. 16—Radial dilatation vs. position: predictions of the models for the [Shima et al. \(1987\)](#) specimen